Small-Signal Analysis of Oscillators Using Generalized Multitime Partial Differential Equations

Ting Mei, *Student Member, IEEE*, and Jaijeet Roychowdhury, *Member, IEEE*

***Abstract*—Standard small-signal analysis methods for circuits break down for oscillators because small-input perturbations result in arbitrarily large-output changes, thus invalidating fundamental assumptions for small-signal analysis. In this paper, we propose a novel oscillator ac approach remedying this situation, thus restoring validity and rigour to small-signal analysis of oscillators. Our approach centers around a novel general equation formulation for circuits that we term the Generalized Multitime Partial Differential Equations (GeMPDE). While this formulation is broadly applicable to any kind of circuit or dynamical system, we show that it has unique advantages for oscillators in that small-input perturbations now lead to small output ones, thus making small-signal analysis valid. A key feature of our approach is to solve for bivariate-frequency variables with the help of novel augmenting-phase-condition equations. Unlike prior oscillator-analysis methods, which require special handling of the phase mode, our GeMPDE-based small-signal analysis provides both amplitude and frequency characteristics in a unified manner and is applicable to any kind of oscillator described by differential equations. We obtain speedups of 1–2 orders of magnitude over the transient-simulation approach commonly used today by designers for oscillator-perturbation analysis.**

***Index Terms*—Generalized Multitime Partial Differential Equations (GeMPDE), oscillator ac analysis, small-signal analysis.**

I. Introduction

OSCILLATORS are building blocks in electronic, mechanical, optical, and many other types of engineering systems—examples include voltage-controlled oscillators, digital clocks, phase-locked loops, motors, engines, lasers, etc. Analysis of the effects of small perturbations on oscillators is an important practical and theoretical problem. Small perturbations can, for example, lead to thickening of the oscillator's frequency spectrum (an effect known as phase noise) or to uncertainties in the locations of switching edges (known as timing jitter) in clocked systems. Effects of such nonidealities include degradation of throughput and bit-error rate in communication systems and the need for lower clock speeds in computer systems.

In recent years, the sources of perturbations to oscillator-based systems have grown in variety. In addition to intrinsic device noise perturbations, interference "noise" from imperfect power-supply/ground lines and chip substrates have become of substantial concern for designers. Correct and speedy analysis of oscillators under small perturbations has therefore become of particular topical importance.

A. Small-Signal Analysis of Oscillators

For nonoscillatory circuits, small-signal linearized analysis ("AC analysis") [1], [2] is a useful and fast means for designers to gain insight into the circuit operation. Because ac analysis provides information about the circuit's long-term response to small periodic inputs via efficient frequency-domain computations, time-consuming transient analysis is not necessary. AC analysis has long been used to efficiently analyze sinusoidal (or periodic) steady-state responses of linear time-invariant (LTI) circuits. AC analyses are a staple for analog designers, who apply it to circuits such as amplifiers, first linearizing the nonlinear circuits about a dc operating point. The concept of ac analysis has also been profitably extended to nonlinear circuits operating in large-signal periodic steady state, such as mixers and switched-capacitor filters (e.g., [3]–[6]). This linear periodic time-varying (LPTV) ac analysis can capture important aspects of periodically driven circuits, such as frequency translation and sampling.

A similar capability for oscillators for, e.g., finding small changes in oscillator frequency caused by an external input, is therefore very desirable. However, as we explain in this paper, neither LTI nor LPTV AC analysis is applicable to oscillators; if applied blindly, breakdown due to ill-conditioning or outright singularity of the ac matrices results. The reason is that oscillators are different from most other electronic circuits in that even small-input perturbations lead to, over time, large changes in phase and timing properties [7]. The fundamental reason for this qualitative difference (between oscillators and, say, amplifiers) can be traced to the fact that all oscillators feature neutral-phase stability—i.e., any periodic solution of an oscillator, if time-shifted by an arbitrarily delay, is also a valid solution.[1] Because of this property, there is no restoring mechanism that corrects errors in phase caused by small perturbations with the result that phase errors can accumulate without bound over time under the influence of a sustained (but arbitrarily small) perturbation. The numerical manifestation of this fundamental property of oscillators is ill-conditioning and singularity of small-signal-analysis matrices.

Manuscript received December 23, 2005; revised April 30, 2006. This work was supported in part by Sandia National Laboratories, in part by the Semiconductor Research Corporation, and in part by the National Science Foundation under Award CCR-0312079. This paper was recommended by Associate Editor J. R. Phillips.

The authors are with the Electrical and Computer Engineering Department, University of Minnesota, Minneapolis, MN 55455 USA (e-mail: meiting@umn.edu; jrg@umn.edu).

Digital Object Identifier 10.1109/TCAD.2006.885826

[1]For this reason, oscillators are said to have no time reference.

B. Previous Work

In the absence of the "usual" small-signal-analysis capability of SPICE, designers are currently forced to resort to full transient analysis for oscillator simulations. However, as is well known [8], transient analysis has disadvantages peculiar to oscillators. Fundamentally, the tradeoff between accuracy of results and step-size is much worse for oscillators than for nonoscillatory circuits like amplifiers and mixers. In particular, small numerical errors in phase accumulate without limit in oscillators, resulting in unacceptable accuracy unless extremely small timesteps ($\sim$400–1000 timesteps per cycle, typically, for a simulation length of $\sim$100 cycles) are taken. This makes transient simulation very much slower than a potential ac analysis, especially when frequency sweeps are desired: for transient, an entire nonlinear simulation is required for each frequency (followed by postprocessing), while the single complex-matrix solution of ac analysis provides the same information more accurately. Therefore, it is very desirable to restore validity and rigour to small-signal analysis for oscillators.

Special techniques have been devised to overcome the ill-conditioning problem in oscillators (e.g., [7], [9], and [10]). The best approach, to our knowledge, is a nonlinear-perturbation approach presented in [7], designed primarily for the phase components of the oscillator. Recent extensions [8] deflate away that part of the input that causes phase variations and, then, apply Floquet theoretic techniques to compute amplitude components. Deflation of phase components ameliorates the singularity problem; however, the method is still susceptible to ill-conditioning caused by imperfect numerical cancellation [7], [11]. Computationally, full Floquet decomposition can be expensive as system sizes increase; techniques based on partial decomposition using Krylov subspace methods, while substantially faster, exacerbate the imperfect-cancellation issue and while still not providing the full response from all amplitude modes.

C. Contributions of This Work

The method proposed in this paper has its roots in a class of techniques based on the concept of multitime partial differential equations (MPDEs), which were proposed and used to efficiently simulate systems with widely separated time scales, i.e., with fast/slow characteristics. In the MPDE formulation, signal components with different rates of variation are represented by their "own" artificial time variables [12], [13]. An extension (the Warped MPDE or WaMPDE) of MPDE methods has also been proposed [14] that is able to better analyze amplitude and frequency modulation (FM) in oscillators. In the WaMPDE, some "warped" time scales are dynamically rescaled, essentially in order to make the undulations of FM signals uniform so that they can be sampled efficiently. The concept of time warping introduced in the WaMPDE was further generalized [14] to obtain a family of equation formulations collectively termed the Generalized MPDE or GeMPDE. A key characteristic of the GeMPDE is that it features "local frequency" variables, which are themselves functions of multiple time scales. These local frequencies are linked to multitime "phase variables" through nonlinear implicit ordinary differential equations (ODEs).

In this paper, we propose a novel and unified approach for small signal or "ac" analysis of oscillators by exploiting a special case of the GeMPDE. In this particular GeMPDE formulation, the frequency is treated as an extra explicit variable with two time scales—an internal "warped" scale and an external "unwarped" time scale. A set of extra equations, which we term phase conditions, are proposed and added to the system to make the numbers of equations and unknowns the same, thus making it possible to obtain a unique solution. One of the effects of using this bivariate-frequency variable is to separate changes in amplitude and frequency, both of which always remain small if the external perturbation is small.[2] Therefore, linear small-signal analysis of this special GeMPDE becomes valid. The numerical manifestation of this fact is a well-posed Jacobian matrix that remains comfortably nonsingular at all frequencies, as we prove.

By restoring validity to small-signal analysis of oscillators with the GeMPDE formulation, our method achieves large speedups over transient solution, just as traditional ac analysis does for nonoscillatory systems. While our linearized-oscillator analysis relies on multitime computations for all the "hard work," "normal" time-domain waveforms are easily recovered through simple and fast postprocessing. The postprocessing step involves the solution of a scalar nonlinear ODE that relates multitime frequency and single-time phase variables. Our method provides both frequency and amplitude variations in a unified manner from the small-signal transfer function calculated and is applicable to any kind of oscillator.

We validate our oscillator ac (OAC) method on a variety of LC and ring oscillators. OAC-analysis results show excellent agreement with carefully run full transient simulations, as expected but provide speedups of 1–2 orders of magnitude. We also demonstrate how OAC can predict injection locking (injection locking [15], [16] is a phenomenon in which an oscillator's natural frequency changes, under certain conditions, to exactly equal that of a small injected signal). OAC captures this nonlinear phenomenon via the scalar-postprocessing nonlinear-ODE solution that bridges multitime and single-time solutions.

D. Organization of the Paper

The remainder of this paper is organized as follows. In Section II, we review the rank-deficiency problem in the frequency-domain conversion matrix of oscillators for the DAE/MPDE and WaMPDE formulations. In Section III, we propose a well-posed GeMPDE formulation and novel augmenting-phase conditions. We also prove the nonsingularity of GeMPDE's linearization and present the OAC technique in this section. In Section IV, we apply OAC to a number of oscillator circuits and demonstrate improvements in computation time over transient, as well as its ability to predict injection locking.

[2] "Small perturbation" actually means that the input and responses should be in a range appropriate for linearization to be valid. For example, if a circuit is only weakly nonlinear, the input can be relatively large.

II. Rank Deficiency in Previous Oscillator Linearization Approaches

Standard small-signal analysis is not applicable to oscillators because of their fundamental property of neutral-phase stability, resulting in singular small-signal matrices [7], [17], [18]. In this section, we first demonstrate the rank-deficiency problem in the DAE/MPDE frequency-domain conversion matrix of oscillators. We then demonstrate how the WaMPDE formulation [14] succeeds in correcting the problem at dc but fails to do so at all other harmonics (we will then go on to show, in Section III, that the GeMPDE-based approach we present here alleviates the problem completely, i.e., at all frequencies).

A. Preliminaries

Oscillator circuits under perturbation can be described by the DAE system

$$\frac{dq(x)}{dt} + f(x) = Au(t) \tag{1}$$

where $u(t)$ is a small-perturbation signal, $x(t)$ is a vector of circuit unknowns (node voltages and branch currents), and A is an incidence matrix that captures the connection of the perturbation to the circuit. It has been shown in [7] that small perturbations applied to orbitally stable oscillators can lead to dramatic changes in output, thus invalidating the fundamental assumption of small-signal analysis, i.e., that output changes always remain small.

To more conveniently perform small-signal analysis of oscillators, we first recall the MPDE [12], [13] forms of (1), which separate the input and system time scales. This leads to a form of the linear time-varying transfer function useful for small-signal analysis, as we show shortly. The MPDE form of (1) is

$$\left[\frac{\partial}{\partial t_1} + \frac{\partial}{\partial t_2}\right] q\left(\hat{x}(t_1,t_2)\right) + f\left(\hat{x}(t_1,t_2)\right) = Au(t_1) \tag{2}$$

where $\hat{x}(t_1,t_2)$ is the bivariate form of $x(t)$ in (1).

We will also need the WaMPDE formulation [14], an extension of the MPDE originally proposed to address efficiency problems the MPDE faces when encountering strong FM in oscillators. Following [14], the WaMPDE corresponding to (1) is

$$\left[\frac{\partial}{\partial t_1} + \omega(t_1)\frac{\partial}{\partial t_2}\right] q(\hat{x}) + f(\hat{x}) = Au(t_1) \tag{3}$$

where $\omega(t_1)$ is a local-frequency variable, which is a function of the unwarped time scale t_1. t_2 is a dynamically rescaled (warped) time scale, which makes the undulation of FM uniform. Using the WaMPDE form separates changes in amplitude and frequency and, as will become clearer shortly, helps alleviate the rank-deficiency problem in the frequency-domain small-signal analysis matrix of oscillators to some extent.

B. Singularity of the MPDE Conversion Matrix at Frequencies $s = i\jmath\omega_0, \forall i$

We assume that $x^*(t_2)$ is the unperturbed steady-state oscillatory solution of (2), i.e., the solution when $u(t_1) = 0$. Linearizing the MPDE (2) around $x^*(t_2)$, we obtain

$$\left[\frac{\partial}{\partial t_1} + \frac{\partial}{\partial t_2}\right](C(t_2)\Delta\hat{x}(t_1,t_2)) + G(t_2)\Delta\hat{x}(t_1,t_2) = Au(t_1). \tag{4}$$

Here, $C(t_2) = (\partial q(\hat{x})/\partial\hat{x})|_{x^*}$ and $G(t_2) = (\partial f(\hat{x})/\partial\hat{x})|_{x^*}$. Performing a Laplace transform with respect to t_1, we further obtain

$$\left[s + \frac{\partial}{\partial t_2}\right](C(t_2)\Delta\hat{x}(t_1,t_2)) + G(t_2)\Delta\hat{x}(t_1,t_2) = AU(s). \tag{5}$$

We can expand the t_2 dependence in a Fourier series, and using the Toeplitz matrix ($\mathbb{T}$) and vector $\overset{\text{FD}}{\mathbb{V}}$ terminology from [11], we obtain a convenient matrix representation for the time-varying small-signal transfer function of the oscillator [17], [19]

$$\underbrace{\left[\overset{\text{FD}}{\Omega}(s)\mathbb{T}_{C(t_2)} + \mathbb{T}_{G(t_2)}\right]}_{\overset{\text{HB}}{\mathbb{J}}(s)} \overset{\text{FD}}{\mathbb{V}}_{\Delta X}(s) = \overset{\text{FD}}{\mathbb{V}}_{A}\, U(s) \tag{6}$$

where

$$\mathbb{T}_{C(t_2)} = \begin{pmatrix} \vdots & \vdots & \vdots & \vdots & \\ \cdots & C_0 & C_{-1} & C_{-2} & \cdots \\ \cdots & C_1 & C_0 & C_{-1} & \cdots \\ \cdots & C_2 & C_1 & C_0 & \cdots \\ & \vdots & \vdots & \vdots & \end{pmatrix}$$

$$\mathbb{T}_{G(t_2)} = \begin{pmatrix} \vdots & \vdots & \vdots & \vdots & \\ \cdots & G_0 & G_{-1} & G_{-2} & \cdots \\ \cdots & G_1 & G_0 & G_{-1} & \cdots \\ \cdots & G_2 & G_1 & G_0 & \cdots \\ & \vdots & \vdots & \vdots & \end{pmatrix}$$

$$\overset{\text{FD}}{\Omega} = \jmath\omega_0 \begin{pmatrix} \ddots & & & & \\ & -I & & & \\ & & 0I & & \\ & & & I & \\ & & & & \ddots \end{pmatrix}$$

$$\overset{\text{FD}}{\Omega}(s) = \overset{\text{FD}}{\Omega} + sI$$

$$\overset{\text{FD}}{\mathbb{V}}_{\Delta X}(s) = \left[\ldots, \Delta X_{-1}^{\mathrm{T}}, \Delta X_0^{\mathrm{T}}, \Delta X_1^{\mathrm{T}}, \ldots\right]^{\mathrm{T}}$$

$$\text{and} \quad \overset{\text{FD}}{\mathbb{V}}_{A} = [\ldots, 0, A^{\mathrm{T}}, 0, \ldots]^{\mathrm{T}} \tag{7}$$

where $\overset{\text{HB}}{\mathbb{J}}(s)$ is often called the frequency-domain conversion matrix [17], [19].

Lemma 2.1: $\overset{\text{HB}}{\mathbb{J}}(s)$ loses rank by 1 $\forall s = i\jmath\omega_0$, where ω_0 is the frequency of a free-running oscillator.

Proof: See the Appendix. ■

This implies that $\overset{\text{HB}}{\mathbb{J}}(s)$ is singular at dc and every harmonic. Note that at dc (i.e., $s=0$), $\overset{\text{HB}}{\mathbb{J}}(0)$ is actually the steady-state Jacobian of harmonic balance (HB) [20].

C. WaMPDE Restores Full Rank to Conversion Matrix at DC

In the WaMPDE formulation, $\hat{x}$ captures the amplitude of circuit unknowns and $\omega(t_1)$ (the "local frequency") captures frequency changes explicitly and separately from the amplitude components. We assume that (3) has an unperturbed steady-state solution $(x^*(t_2), \omega_0)$. Linearization of (3) around (x^*, ω_0) yields

$$\left[\frac{\partial}{\partial t_1}+\omega_0\frac{\partial}{\partial t_2}\right](C(t_2)\Delta\hat{x}(t_1,t_2))+G(t_2)\Delta\hat{x}(t_1,t_2) + \Delta\omega(t_1)\frac{\partial}{\partial t_2}q(x^*)=Au(t_1). \quad (8)$$

Following the same procedure as in Section II-B, we obtain a frequency-domain discretized system

$$\underbrace{\left[\left(\overset{\text{FD}}{\Omega}(s)\mathbb{T}_{C(t_2)}+\mathbb{T}_{G(t_2)}\right),\overset{\text{FD}}{\mathbb{V}}_{\dot{q}^*(t_2)}\right]}_{\overset{\text{HB}}{\mathbb{J}}_{A(s)}}\begin{pmatrix}\overset{\text{FD}}{\mathbb{V}}_{\Delta X}(s)\\ \Delta\omega(s)\end{pmatrix} = \overset{\text{FD}}{\mathbb{V}}_{A}U(s) \quad (9)$$

where $\overset{\text{HB}}{\mathbb{J}}_{A}(s)$ is the augmented HB Jacobian with offset s (or augmented conversion matrix). Compared with (6), $\overset{\text{HB}}{\mathbb{J}}_{A}(s)$ is augmented with the right column $\overset{\text{FD}}{\mathbb{V}}_{\dot{q}^*(t)}$.

Lemma 2.2: Augmenting $\overset{\text{HB}}{\mathbb{J}}(s)$ by a column $\overset{\text{FD}}{\mathbb{V}}_{\dot{q}^*(t)}$ ($\overset{\text{HB}}{\mathbb{J}}_{A}(s)$) restores full rank only in the case $s=0$.

Proof: See the Appendix. ■

Note that at $s=\text{DC}$, $\overset{\text{HB}}{\mathbb{J}}_{A}(s)$ with an appropriate phase-condition row is actually the steady-state Jacobian for oscillator HB [18], [20]. It is because this matrix is nonsingular that HB can solve for the oscillator's steady state.

III. Small-Signal Linearization of the GeMPDE

For valid small-signal analysis, it is essential that the Jacobian matrix is full rank at all frequencies. In this section, we propose a special GeMPDE formulation and prove that it solves the rank-deficiency problem of the Jacobian matrix completely with the use of new phase conditions. We first obtain a new small-signal transfer function under this formulation, and then, show how both phase/frequency and amplitude characteristics of oscillators can be easily recovered from multitime solutions.

A. GeMPDE Formulation

The GeMPDE, outlined in [14], is

$$\left[\hat{\Omega}(t_1,\ldots,t_d)\cdot\left[\frac{\partial}{\partial t_1},\ldots,\frac{\partial}{\partial t_d}\right]\right]q(\hat{x}(t_1,\ldots,t_d)) + f(\hat{x}(t_1,\ldots,t_d))=\hat{b}(t_1,\ldots,t_d) \quad (10)$$

where d is the number of artificial time scales, the "phase" functions $\hat{\Phi}(t_1,\ldots,t_d)$ and the "local-frequency" functions $\hat{\Omega}(\tau_1,\ldots,\tau_d)$ are defined as

$$\hat{\Phi}(t_1,\ldots,t_d)=\begin{pmatrix}\tau_1\\ \vdots\\ \tau_d\end{pmatrix} = \begin{pmatrix}\hat{\phi}_1(t_1,\ldots,t_d)\\ \vdots\\ \hat{\phi}_1(t_1,\ldots,t_d)\end{pmatrix} \quad (11)$$

$$\hat{\Omega}(\tau_1,\ldots,\tau_d)=\begin{pmatrix}\hat{\omega}_1(\tau_1,\ldots,\tau_d)\\ \vdots\\ \hat{\omega}_1(\tau_1,\ldots,\tau_d)\end{pmatrix} \quad (12)$$

where $\hat{\Phi}$ and $\hat{\Omega}$ is related by a nonlinear implicit ODE

$$\left(\frac{\partial}{\partial t_1}+\cdots+\frac{\partial}{\partial t_d}\right)\hat{\Phi}(t_1,\ldots,t_d)=\hat{\Omega}\left(\hat{\Phi}(t_1,\ldots,t_d)\right). \quad (13)$$

This relation is the generalization of the fact that phase is the integral of local frequency.

Theorem 3.1: If $(\hat{\Omega},\hat{x})$ is a solution of (10), then the one-time waveform defined by $x(t)=\hat{x}(\hat{\Phi}(t,\ldots,t))$ solves the underlying DAE system, if $b(t)=\hat{b}(\hat{\Phi}(t,\ldots,t))$.

Proof: See [14]. ■

B. Small-Signal Linearization of the GeMPDE

To facilitate small-signal analysis, we use a special case of the GeMPDE. In this particular GeMPDE formulation, the frequency ω is treated as an extra explicit variable that is a function of two time scales: an internal warped time scale (t_1) and an external unwarped time scale (t_2). The special bivariate GeMPDE form of (1) is

$$\left[\frac{\partial}{\partial t_1}+\hat{\omega}(t_1,t_2)\frac{\partial}{\partial t_2}\right]q(\hat{x}(t_1,t_2)) + f(\hat{x}(t_1,t_2))=b(t)=Au(t_1). \quad (14)$$

Lemma 3.1: If $(\hat{\omega},\hat{x})$ is a solution of (14), then the one-time waveform defined by $x(t)=\hat{x}(t,\hat{\phi}(t,t))$ solves the underlying DAE system if $b(t)=\hat{b}(t,\hat{\phi}(t,t))$, where $\hat{\phi}$ and $\hat{\omega}$ are related by

$$\frac{\partial\hat{\phi}(t,t)}{\partial t}=\frac{\partial\hat{\phi}(\tau_1=t,\tau_2=t)}{\partial\tau_1}+\frac{\partial\hat{\phi}(\tau_1=t,\tau_2=t)}{\partial\tau_2} =\hat{\omega}\left(t,\hat{\phi}(t,t)\right). \quad (15)$$

Proof: See the Appendix. ■

Defining $\phi(t)=\hat{\phi}(t,t)$, we can rewrite the phase-frequency relation (15) as

$$\frac{d\phi(t)}{dt}=\hat{\omega}\left(t,\phi(t)\right). \quad (16)$$

This equation relates the multitime frequency and the single-time phase variable. The single-time phase is then used to obtain a single-time solution from MPDE solutions using Lemma 3.1.

We now linearize this special case of the GeMPDE. We first note that the unperturbed steady-state solution of the WaMPDE (3) $(x^*(t_2), \omega_0)$ also solves the GeMPDE (14). We can then linearize (14) around $(x^*(t_2), \omega_0)$ to obtain the linearized GeMPDE:

$$\left[\frac{\partial}{\partial t_1} + (\omega_0 + \Delta\omega(t_1,t_2))\frac{\partial}{\partial t_2}\right] q\left(x^* + \Delta\hat{x}(t_1,t_2)\right) + f\left(x^* + \Delta\hat{x}(t_1,t_2)\right) = Au(t_1) \quad (17)$$

i.e.,

$$\left[\frac{\partial}{\partial t_1} + \omega_0\frac{\partial}{\partial t_2}\right](C(t_2)\Delta\hat{x}(t_1,t_2)) + G(t_2)\Delta\hat{x}(t_1,t_2) + \Delta\omega(t_1,t_2)\frac{\partial}{\partial t_2}q(x^*) = Au(t_1). \quad (18)$$

Following the same procedure as in Section II-B, we continue to obtain a frequency-domain discretized system

$$\underbrace{\left[\left(\overset{\mathrm{FD}}{\Omega}(s)\mathbb{T}_{C(t_2)} + \mathbb{T}_{G(t_2)}\right), \mathbb{T}_{\dot{q}^*(t_2)}\right]}_{\overset{\mathrm{HB}}{\mathbb{J}}_{\mathrm{Ge}(s)}} \begin{pmatrix} \overset{\mathrm{FD}}{\mathbb{V}}_{\Delta X}(s) \\ \overset{\mathrm{FD}}{\mathbb{V}}_{\Delta}\,\omega(s) \end{pmatrix} = \overset{\mathrm{FD}}{\mathbb{V}}_{A}\,U(s). \quad (19)$$

Comparing with (9), we note that now the Jacobian is augmented by several more columns (N columns of $\mathbb{T}_{\dot{q}^*(t_2)}$, where N is the number of harmonics used in our truncated Fourier series). In this case, the size of $\overset{\mathrm{HB}}{\mathbb{J}}_{\mathrm{Ge}}(s)$ is $nN \times (n+1)N$, where n is the number of circuit unknowns.

Lemma 3.2: The augmented matrix $\overset{\mathrm{HB}}{\mathbb{J}}_{\mathrm{Ge}}(s)$ (augmenting $\overset{\mathrm{HB}}{\mathbb{J}}(s)$ by columns of $\mathbb{T}_{\dot{q}^*(t_2)}$) is full rank at all frequencies.

Proof: See the Appendix. ■

This implies that $\overset{\mathrm{HB}}{\mathbb{J}}_{\mathrm{Ge}}(s)$, if properly augmented with linearly independent rows (as shown in the following), can be nonsingular at all frequencies. As a result, if the perturbation signal is small, then both $\overset{\mathrm{FD}}{\mathbb{V}}_{\Delta X}(s)$ and $\overset{\mathrm{FD}}{\mathbb{V}}_{\Delta\omega}(s)$ remain small, making linear small-signal analysis of this special GeMPDE valid.

C. New Phase Conditions

Since we have augmented $\overset{\mathrm{HB}}{\mathbb{J}}(s)$ by N columns above, we have N more unknowns than equations. We require N more equations in order to obtain a unique solution. We will term these equations phase conditions. While there is considerable apparent freedom in choosing phase conditions, they need to satisfy a number of conditions in order to be useful from the standpoint of small-signal analysis. In particular, the phase-condition rows that augment $\overset{\mathrm{HB}}{\mathbb{J}}_{\mathrm{Ge}}(s)$: 1) must be full rank themselves and 2) in addition make the entire augmented Jacobian matrix full rank.

We now propose the following phase-condition equations to satisfy these characteristics:

$$\omega(t_1,t_2)\frac{\partial}{\partial t_2}\hat{x}_l = \frac{\partial x_{ls}(t_2)}{\partial t_2} \quad (20)$$

where l is a fixed integer. $\hat{x}_l$ denotes the lth element of $\hat{x}$, while x_{ls} is the lth element of the steady-state solution $x_s(t_2)$.

It is interesting to note that these phase conditions (20) are a generalization of

$$\omega_0\frac{dx_l}{dt_2}|_{t_2=0} = 0 \quad (21)$$

a phase condition standardly used in oscillator steady-state methods [14]. The physical meaning of this phase condition is that the unknown x_l has a zero derivative at $t_2 = 0$ at the steady state. In steady-state methods, the equation system of an oscillator has only one extra unknown, the oscillator's frequency. Thus, only one augmenting-phase-condition equation is required to make the system "square." Also, the use of a scalar ω_0 within the phase equation is not important since the right-hand sized is zero (however, this is not true for GeMPDE formulations).

In our GeMPDE formulation, there are N extra unknowns due to the fact that $\omega(t_1,t_2)$ is a function depending on both t_1 and t_2 (N is the number of terms in the truncated Fourier series). The phase condition is therefore generalized by equating the scaled derivative of x_l to that of x_l at the steady state for N points (i.e., for $t_{2i} = (i-1)/(N)T_2, i = 1, 2, \ldots, N$). Here, $\omega(t_1,t_2)$ cannot be omitted, since the right-hand side is not zero. The simple phase-condition equation used in steady-state methods becomes a special case of the GeMPDE phase condition.

Note that, just as for the steady-state case, the choice of the phase-condition variable x_l should be dictated by physical intuition about the oscillator. For example, choosing x_l to correspond to a dc voltage source (e.g., the power supply) is inappropriate, since its waveform is constant with time and (20) will lead to degeneracy and rank-deficiency in the GeMPDE small-signal matrix. On the other hand, e.g., the capacitor voltage or the inductor current in an LC oscillator are excellent choices, since they have periodic time-varying waveforms.

It is obvious that the unperturbed steady state $(x_l^*(t_2), \omega_0)$ satisfies (20). By linearizing around (x_l^*, ω_0) and expanding the t_2 dependence in Fourier series, we obtain

$$\underbrace{\left[\overset{\mathrm{FD}}{\Omega}\,\mathbb{T}_{e_l^T}, \mathbb{T}_{\dot{x}_l^*(t_2)}\right]}_{P} \begin{pmatrix} \overset{\mathrm{FD}}{\mathbb{V}}_{\Delta X}(s) \\ \overset{\mathrm{FD}}{\mathbb{V}}_{\Delta\omega}(s) \end{pmatrix} = 0. \quad (22)$$

Lemma 3.3: The phase-condition submatrix P is full rank at all frequencies.

Proof: See the Appendix. ■

This implies that the phase-condition rows that augment $\overset{\mathrm{HB}}{\mathbb{J}}_{\mathrm{Ge}}(s)$ is full rank.

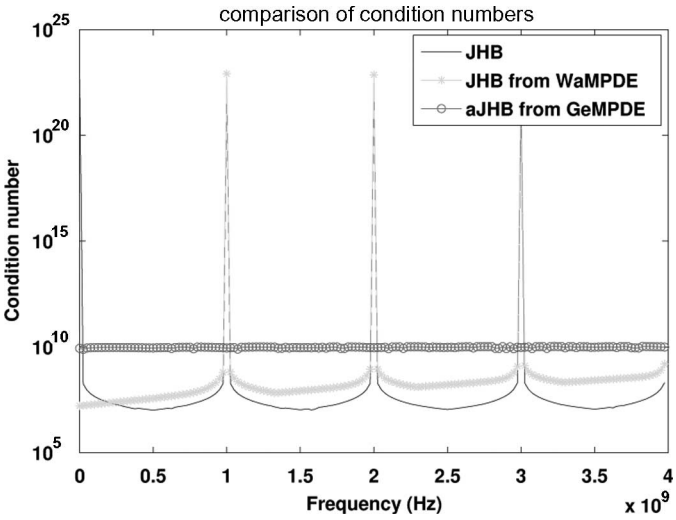

Fig. 1. Condition numbers: Original Jacobian matrix (solid line), augmented Jacobian from WaMPDE (*), and augmented Jacobian from GeMPDE (o). The frequency of LC oscillator is 1591.5 Hz. A total of $N = 61$ harmonics were used.

Putting the phase conditions and GeMPDE together, we obtain

$$\begin{bmatrix} \begin{pmatrix} \overset{\mathrm{FD}}{\Omega}(s)\mathbb{T}_{C(t_2)} + \mathbb{T}_{G(t_2)} \end{pmatrix}, & \mathbb{T}_{\dot{q}^*(t_2)} \\ \overset{\mathrm{FD}}{\Omega}\,\mathbb{T}_{e_l^T}, & \mathbb{T}_{\dot{x}_l^*(t_2)} \end{bmatrix} \begin{pmatrix} \overset{\mathrm{FD}}{\mathbb{V}}_{\Delta X}(s) \\ \overset{\mathrm{FD}}{\mathbb{V}}_{\Delta\omega}(s) \end{pmatrix} = \begin{pmatrix} \overset{\mathrm{FD}}{\mathbb{V}}_A \\ z \end{pmatrix} U(s) \quad (23)$$

where $z = [0, \ldots, 0]^{\mathrm{T}}$. The corresponding small-signal transfer function is

$$\begin{aligned} \overset{\mathrm{FD}}{\mathbb{V}}_H(s) &= \begin{pmatrix} \overset{\mathrm{FD}}{\mathbb{V}}_{\Delta X}(s) \\ \overset{\mathrm{FD}}{\mathbb{V}}_{\Delta\omega}(s) \end{pmatrix} / U(s) \\ &= \begin{bmatrix} \begin{pmatrix} \overset{\mathrm{FD}}{\Omega}(s)\mathbb{T}_{C(t_2)} + \mathbb{T}_{G(t_2)} \end{pmatrix}, & \mathbb{T}_{\dot{q}^*(t_2)} \\ \overset{\mathrm{FD}}{\Omega}\,\mathbb{T}_{e_l^T}, & \mathbb{T}_{\dot{x}_l^*(t_2)} \end{bmatrix}^{-1} \\ &\quad \times \begin{pmatrix} \overset{\mathrm{FD}}{\mathbb{V}}_A \\ z \end{pmatrix}. \end{aligned} \quad (24)$$

Equation (24) is always nonsingular, for all frequencies. This is confirmed by numerical results: Fig. 1 shows condition numbers of the original Jacobian matrix, the augmented Jacobian from the WaMPDE (with one phase condition) and the augmented Jacobian from the GeMPDE (with N phase conditions; N is the number of harmonics), using a simple nonlinear LC oscillator with a negative resistor. As shown, the original Jacobian becomes singular at $s = ijw_0, \forall i$; the WaMPDE corrects the singularity problem only at dc, while the GeMPDE addresses the singularity problem completely at all frequencies.

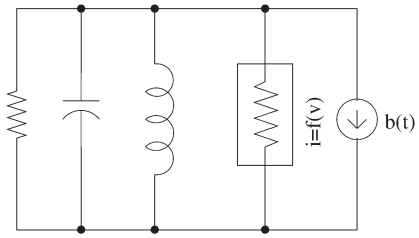

Fig. 2. Simple 1-GHz LC oscillator with a negative resistor.

D. Obtaining Phase and Amplitude Characteristics

Once the transfer function is obtained by (24), we can obtain $\overset{\mathrm{FD}}{\mathbb{V}}_{\Delta X}(s)$ and $\overset{\mathrm{FD}}{\mathbb{V}}_{\Delta\omega}(s)$ by applying perturbations at different frequencies. Multitime waveforms of Δx and $\Delta\omega$ are then obtained by evaluating the Fourier series [using, e.g., the fast Fourier transform (FFT)]. Phase characteristics are recovered by solving the phase-frequency relation [(16)]: To obtain the phase variation from $\Delta\omega$, we linearize (16) around (ϕ_0, ω_0). Using $\phi_0 = \omega_0 t$, we have

$$\frac{d\Delta\phi(t)}{dt} = \hat{\Delta\omega}\left(t, \omega_0 t + \Delta\phi(t)\right). \quad (25)$$

Finally, the one-time form of the amplitude variations $\Delta x(t)$ can be recovered using Lemma 3.1

$$\Delta x(t) = \hat{\Delta x}\left(t, \phi(t)\right) \quad (26)$$

where $\phi(t) = \omega_0 t + \Delta\phi(t)$. The overall solution of the oscillator is given by

$$x(t) = x^*\left(\phi(t)\right) + \hat{\Delta x}\left(t, \phi(t)\right) \quad (27)$$

where x^* is the steady-state oscillatory solution.

In summary, the flow of the autonomous ac analysis process is outlined below:

Flow of oscillator ac algorithm

1) Solve for the steady-state solution (x^*, w_0) using HB or shooting.
2) Calculate the GeMPDE transfer function numerically using (24).
3) Obtain multitime time-domain waveforms of Δx and $\Delta\omega$ at a given frequency (via FFTs or brute-force evaluation of a sum of sinusoidal components).
4) Solve (25) numerically for the phase variation.
5) Solve (26) numerically for the amplitude variations.
6) Finally, generate the overall solution using (27).

E. Using OAC to Predict Injection Locking

Although our method is based on linearization, it can capture injection locking because the scalar phase (25), which is automatically available using our special form of GeMPDE, is nonlinear. When an oscillator locks to the perturbation signal, its phase follows that of the perturbation signal, i.e.,

$$\omega_0 t + \Delta\phi(t) = \omega_1 t + \theta \quad (28)$$

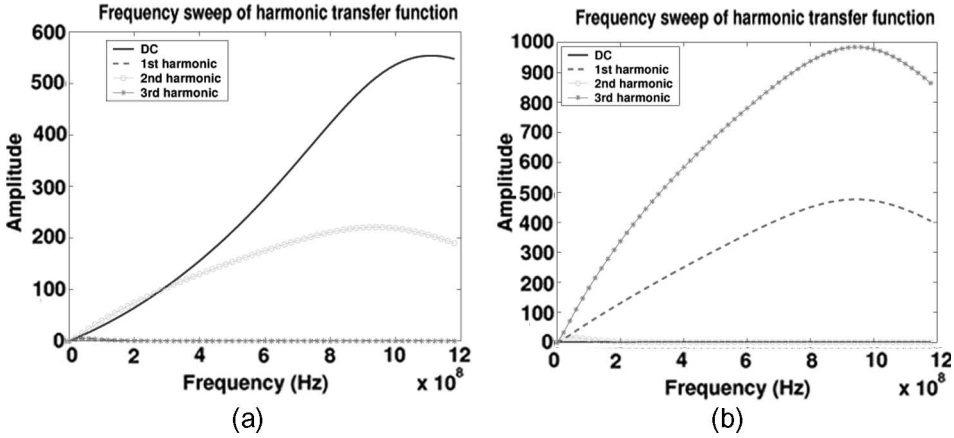

Fig. 3. Harmonic transfer functions: The frequency sweeps from dc to 1.2×10^9 Hz. (a) Harmonic transfer functions of the capacitor voltage. (b) Harmonic transfer functions of the local frequency.

where ω_0 is the frequency of the free-running oscillator, ω_1 is the perturbation frequency, and θ is a constant representing the phase difference between the locked oscillator and the perturbation signal. Hence

$$\Delta\phi(t) = (\omega_1 - \omega_0)t + \theta = \Delta\omega_0 t + \theta. \tag{29}$$

In other words, if the oscillator is in lock, the phase $\Delta\phi(t)$ should change linearly with a slope of $\Delta\omega_0$. By examining the waveform of $\Delta\phi(t)$ obtained from (25), injection locking in oscillators can be easily predicted via our new small-signal analysis.

IV. Application and Validation

In this section, we apply the GeMPDE-based small-signal analysis to LC, ring, and cross-coupled CMOS oscillators. Comparisons with direct SPICE-like transient simulations confirm that our method captures oscillator phase/frequency and amplitude variations correctly. Speedups of orders of magnitude are obtained, however, over SPICE-like transient simulation. We also verify OAC's capability of predicting injection locking in oscillators. All simulations were performed using MATLAB on a 2.4-GHz Athlon XP-based PC running on Linux.

A. One-GHz Negative-Resistance LC Oscillator

A simple 1-GHz LC oscillator with a negative resistor is shown in Fig. 2. At steady state, the amplitude of the inductor current is 1.2 mA.

The circuit is perturbed by a current source in parallel with the inductor. Fig. 3 shows frequency sweeps akin to standard ac analysis, for both the capacitor voltage and the local frequency. The transfer functions for the capacitor voltage represent effects of amplitude modulation (at the capacitor node), while the transfer functions for the local frequency capture FM. The horizontal axis is the frequency of the "input" perturbation signal, just as in LTI AC analysis. As shown, different harmonics of the outputs have different transfer functions, since oscillators are LPTV systems [17], [19]. Note that for the perturbation frequency at the oscillator's natural frequency ω_0, i.e., 1 GHz, all transfer functions have finite values verifying that our GeMPDE-based conversion matrix is nonsingular.

Fig. 4(a) shows the phase variation recovered from the bivariate form of frequency [using (25)] under a perturbation of $4 \times 10^{-5}\ \sin(1.03w_0t)$. For comparison, we also depict the phase variation solved from Floquet-theory-based analysis [7] in Fig. 4(a). The two waveforms have similar shapes but slightly different values—this corresponds to small tweaks in the orbital deviation. Fig. 4(b) shows phase variations solved from both methods for longer simulation time. As shown, the long-range slopes for the linear growth of the phase deviations from both methods do not equal to each other (this may be caused by numerical integration errors during the solution of the phase equation and is under investigation currently).

Both multitime and recovered one-time forms of amplitude variation of the capacitor voltage are shown in Fig. 4(c)–(d). The long-range orbital deviations stay small, as shown in Fig. 4(d). The capacitor-voltage waveform is obtained using (27) and compared with full transient simulation in Fig. 5. As shown, the results from our method match full simulation perfectly. A speedup of 15 times is obtained in this example.

We also test OAC for predicting injection locking, first applying a perturbation of the same frequency as the oscillator's natural frequency ω_0, noting that the phase shift should converge to a constant in this case. We then change the perturbation frequency to $1.03\omega_0$; in this case, we expect the phase to change linearly with a slope of 0.03 (in our implementation, the slope is scaled by $1/\omega_0$, so the slope is $\Delta\omega_0/\omega_0$). The perturbations are increased in strength to ensure that the oscillator is in lock. The phase variations from the small-signal analysis in both cases are shown in Figs. 6 and 7. Transient simulation results are also provided to verify that the oscillator is in lock. As shown in Figs. 6 and 7, the phase variations from our method change as expected.

B. Three-Stage Ring Oscillator

A three-stage ring oscillator with identical stages is shown in Fig. 8. The oscillator has a natural frequency of 1.53×10^5 Hz. The amplitude of the steady-state load current is about 1.2 mA.

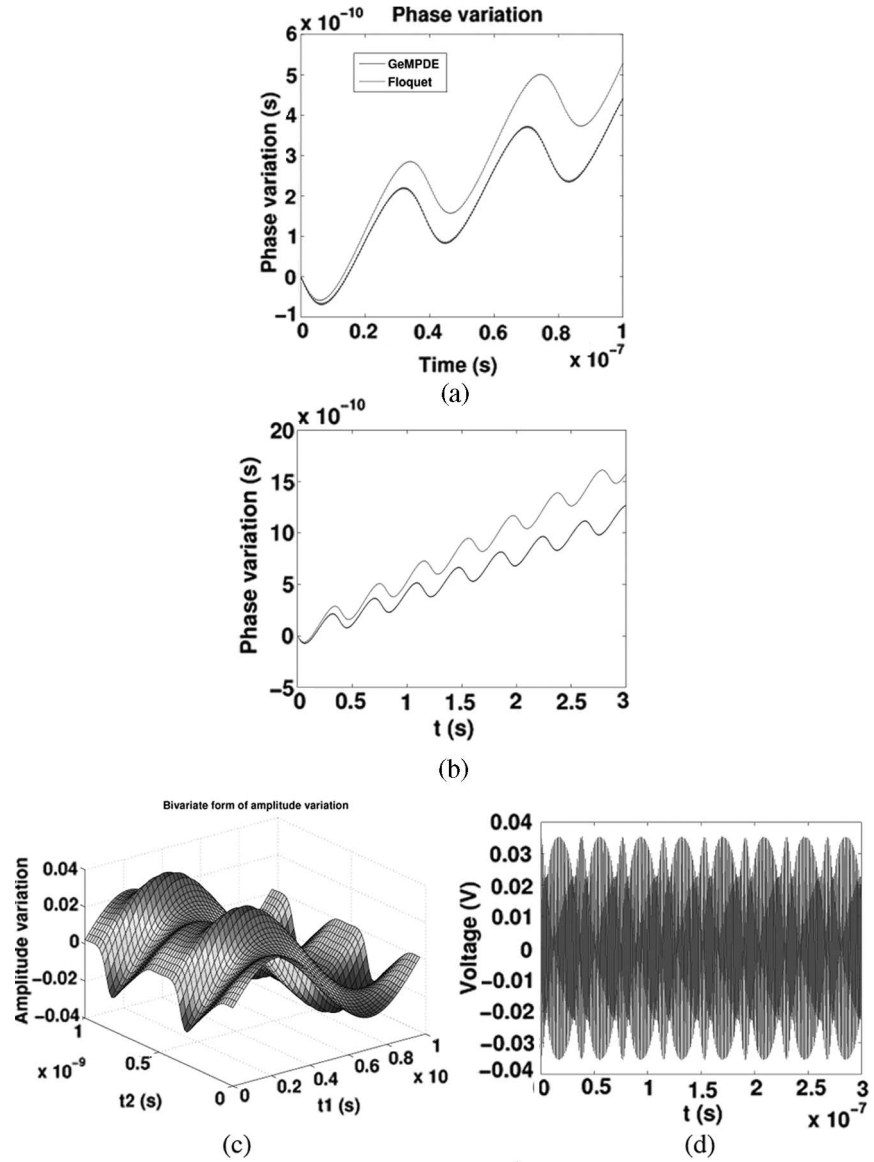

Fig. 4. Phase and amplitude variations of the capacitor voltage when the perturbation current is $4 \times 10^{-5} \sin(1.03 w_0 t)$. The figure shows the simulation result for 100–300 cycles. (a) Comparison: phase variation (100 cycles). (b) Comparison: phase variation (300 cycles). (c) Multitime solution of amplitude variation. (d) One-time solution of amplitude variation (300 cycles).

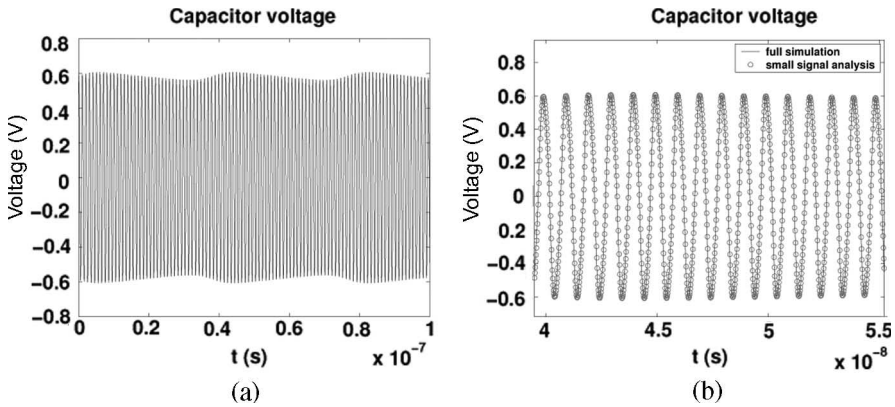

Fig. 5. Comparison of results from small-signal analysis and full transient simulation [the perturbation current is $4 \times 10^{-5} \sin(1.03 w_0 t)$]. (a) Result recovered from small-signal analysis. (b) Detailed comparison (zoom in).

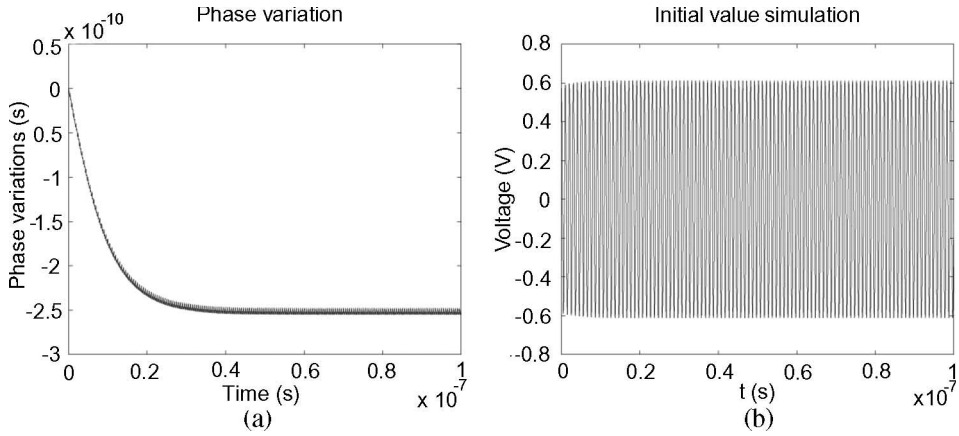

Fig. 6. Oscillator in lock: The perturbation current is $5 \times 10^{-5} \sin(w_0 t)$. The figure shows simulation result for 100 cycles. (a) Phase variation from small-signal analysis. (b) Transient simulation result.

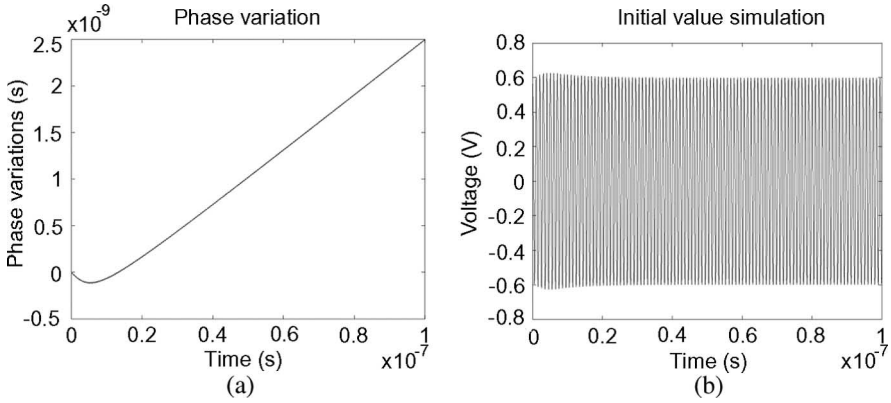

Fig. 7. Oscillator in lock: The perturbation current is $8 \times 10^{-5} \sin(1.03 w_0 t)$. The figure shows simulation result for 100 cycles. (a) Phase variation from small-signal analysis. (b) Transient simulation result.

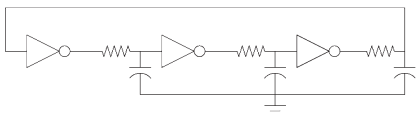

Fig. 8. Three-stage oscillator with identical stages.

Fig. 9 shows ac analysis frequency sweeps for both the capacitor voltage and the local frequency of the oscillator under a perturbation current, which is connected in parallel with the load capacitor at node 1. Note that all transfer functions remain bounded when the perturbation frequency is the oscillator's free-running frequency ω_0, as well as at every harmonic $2\omega_0, 3\omega_0, \ldots$, etc., the harmonics are not depicted in the figure.

Fig. 10 shows the phase and amplitude variations at node 1 (the perturbation current is $5 \times 10^{-5} \sin(1.04 w_0 t)$). The waveform at node 1 is compared with full transient simulation in Fig. 11. Again, we see perfect agreement between results from our method and SPICE-like simulation, with a speedup of 20 in this case.

Fig. 12 shows the simulation result when the oscillator is in lock. Observe that the phase changes linearly, as expected. Transient simulation results are also provided to verify that the oscillator is in lock.

C. Four-GHz Colpitts LC Oscillator

A Colpitts LC oscillator is shown in Fig. 13. The circuit has a free-running frequency of approximately 4 GHz.

We perturb the oscillator with a small sinusoidal voltage source in series with the inductor L1. Fig. 14 shows frequency sweeps for both the current through L1 and the local frequency. All harmonic transfer functions have well-defined finite peaks around the oscillator's natural frequency.

Fig. 15 shows the phase and amplitude variations of the current through L1 when the perturbation current is $2 \times 10^{-3} \sin(1.02 w_0 t)$. The waveform of the current through L1 is compared with full transient simulation in Fig. 16. As shown, results from our method match full simulations perfectly. A speedup of 100 times is obtained in this example. We obtain larger speedups for this circuit as compared to prior ones, since its size is larger.

Fig. 17 shows simulation results when the oscillator is in lock. Again, our method predicts the injection locking correctly, as verified by transient simulation.

D. One-GHz Cross-Coupled CMOS Oscillator

A cross-coupled CMOS oscillator is shown in Fig. 18. The circuit has a free-running frequency of approximately 1 GHz.

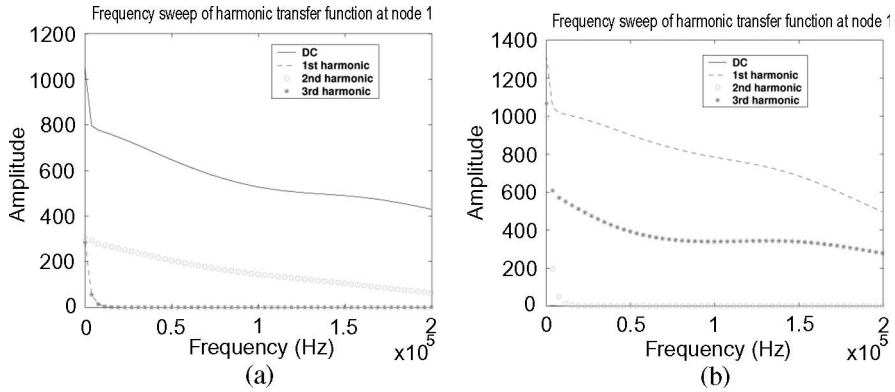

Fig. 9. Harmonic transfer functions: The frequency sweeps from dc to 2×10^5 Hz. (a) Harmonic transfer functions at node 1. (b) Harmonic transfer functions of the local frequency.

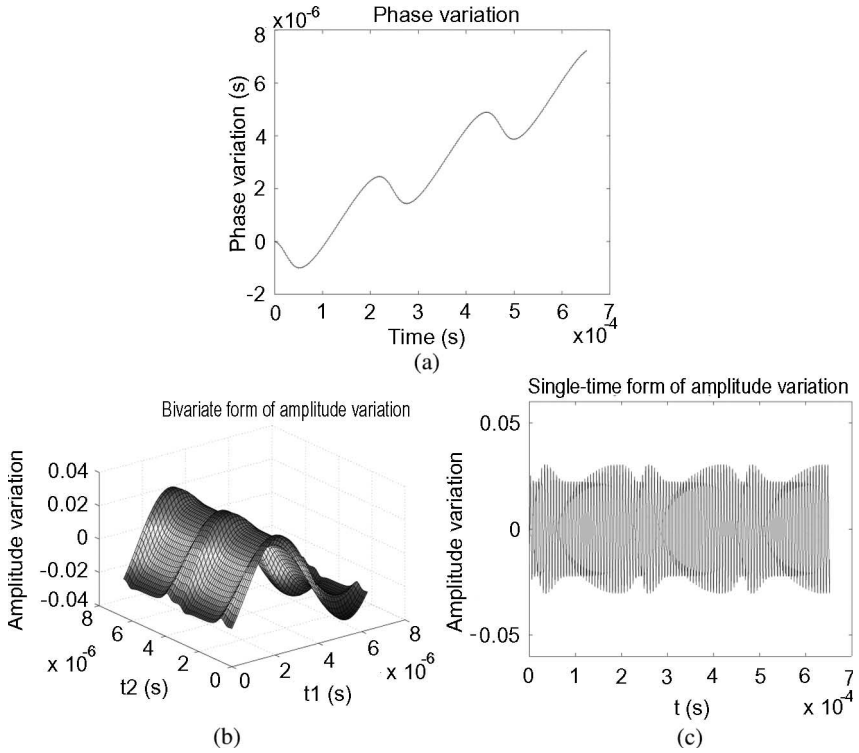

Fig. 10. Phase and amplitude variations of the capacitor voltage when the perturbation current is $5 \times 10^{-5} \sin(1.04 w_0 t)$. The figure shows simulation result for 100 cycles. (a) Phase variation. (b) Multitime solution of amplitude variation. (c) One-time solution of amplitude variation.

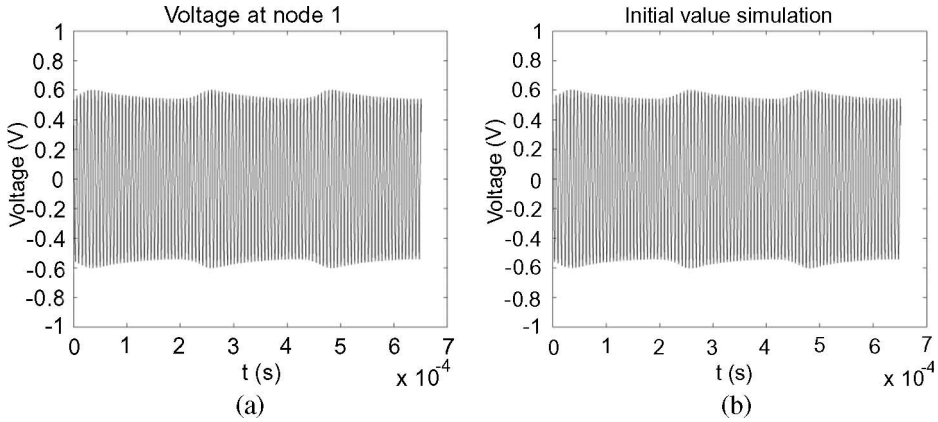

Fig. 11. Comparison of the result from small-signal analysis and full transient simulation [the perturbation current is $5 \times 10^{-5} \sin(1.04 w_0 t)$]. (a) Result recovered from small-signal analysis. (b) Transient simulation result.

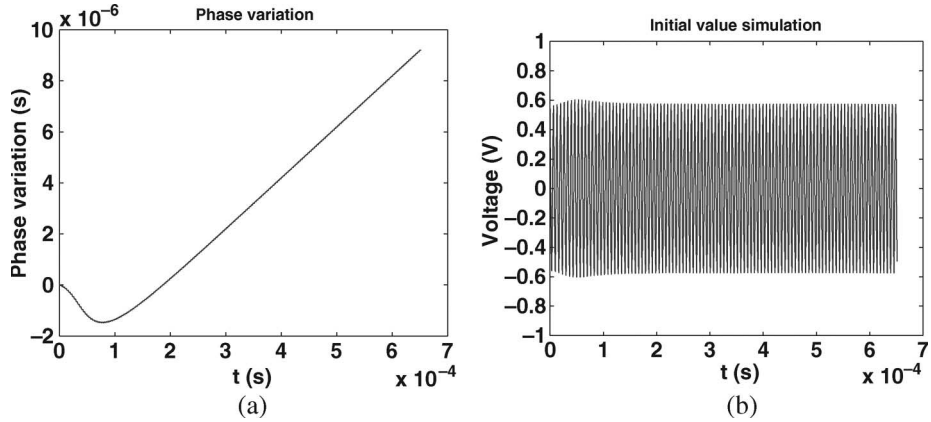

Fig. 12. Oscillator in lock: The perturbation current is $5 \times 10^{-5} \sin(1.02 w_0 t)$. The figure shows simulation result for 100 cycles. (a) Phase variation from small-signal analysis. (b) Transient simulation result.

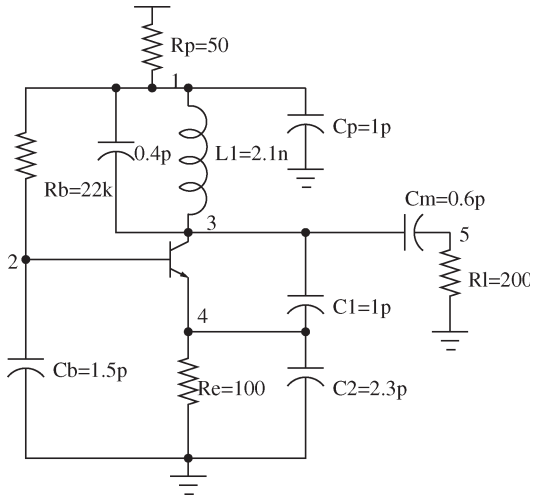

Fig. 13. Four-GHz Colpitts LC oscillator.

We inject a small sinusoidal current to one of the oscillator outputs. Fig. 19 shows frequency sweeps for both the output voltage and the local frequency. Similar to the previous example, all harmonic transfer functions have finite well-defined peaks around the oscillator's natural frequency.

Fig. 20 shows the resulting phase and amplitude variations of the output voltage. The waveform at the output is compared with full transient simulation in Fig. 21. Fig. 22 shows simulation results when the oscillator is in lock. A speedup of 50 times is obtained in this example.

V. Conclusion and Future Directions

We have presented a mathematical formulation and computational algorithms for rigorously valid small-signal analysis of oscillators. Our GeMPDE-based OAC method captures amplitude and frequency variations in oscillators under perturbations accurately and in a unified manner delivering large speedups over the full transient simulations that were the only comprehensive prior alternative. The method operates by splitting up the oscillator small-signal problem into linear computations involving a well-conditioned matrix, followed by solution of a small scalar nonlinear differential equation. The method is also able to predict injection locking in oscillators, an inherently nonlinear phenomenon, because of the latter step.

At this point, we feel that the method is already suitable for evaluation, further development, and deployment by the community and industry. We emphasize, however, that several interesting and important theoretical, as well as practical, issues remain to be explored. These include understanding more precisely the impact of different phase conditions on matrix conditioning, obtaining concrete connections between the positive predictive value perturbation projection vector (PPV) equation for phase derived from Floquet theory [7] and the more general form of GeMPDE phase (20), and performing a stochastic analysis of the linearized GeMPDE to obtain potentially new insights into phase noise and jitter. We are currently investigating these topics.

Appendix

Lemma 2.1: $\overset{\mathrm{HB}}{\mathbb{J}}(s)$ loses rank by one $\forall s = i\jmath\omega_0$, where ω_0 is the frequency of a free-running oscillator.

Proof: For simplicity in exposition, we assume the oscillator is an ODE—extension to the DAE case is straightforward using ideas from [11]. From [11, (19)]

$$(\Omega(s) - \mathbb{T}_M) = \mathbb{T}_{V^{\mathrm{T}}(t)} \overset{\mathrm{HB}}{\mathbb{J}}(s) \mathbb{T}_{U(t)}. \tag{30}$$

Using $V^{\mathrm{T}}(t) = U^{-1}(t)$ (from [11, (5)] except here $C(t) = I$), we have

$$\overset{\mathrm{HB}}{\mathbb{J}}(s) = \mathbb{T}_{U(t)} (\Omega(s) - \mathbb{T}_M) \mathbb{T}^{-1}_{U(t)}. \tag{31}$$

The singularity or nonsingularity of $(\Omega(s) - \mathbb{T}_M)$ is the same as that of $\overset{\mathrm{HB}}{\mathbb{J}}(s)$, because they are related by a similarity transformation.

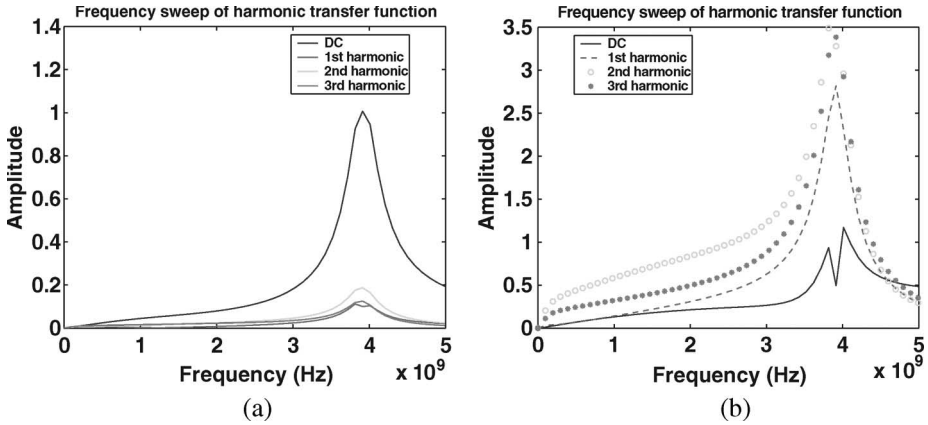

Fig. 14. Harmonic transfer functions: The frequency sweeps from dc to 5×10^9 Hz. (a) Harmonic transfer functions of the current through L1. (b) Harmonic transfer functions of the local frequency.

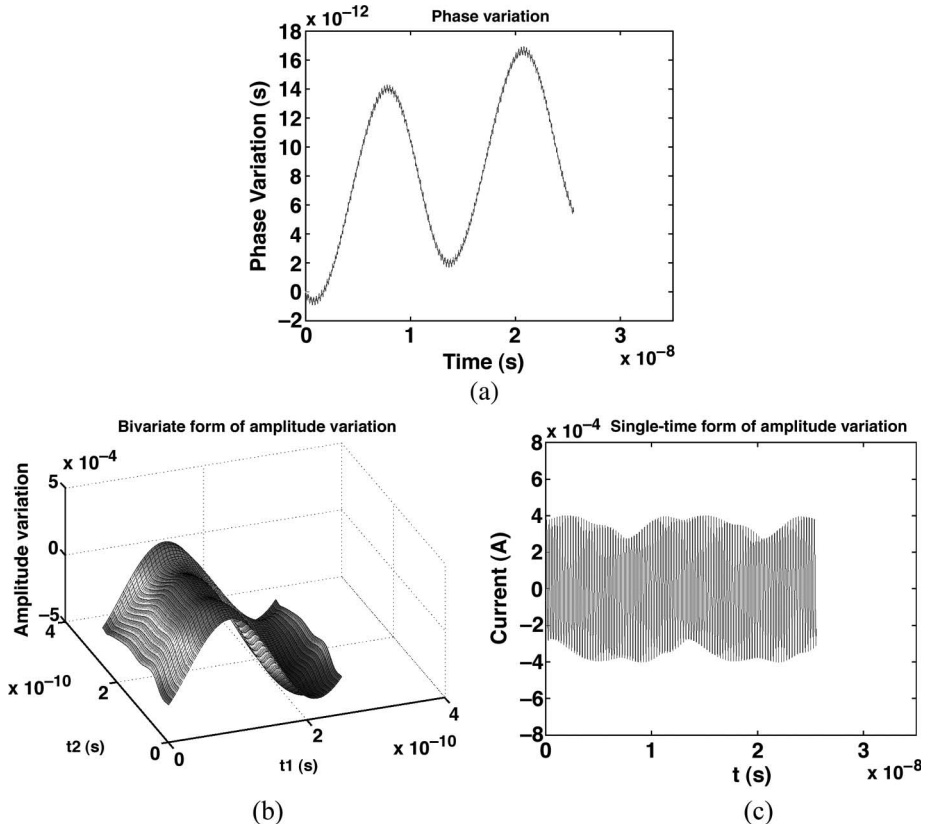

Fig. 15. Phase and amplitude variations of the current through L1 when the perturbation current is $2 \times 10^{-3} \sin(1.02 w_0 t)$. The figure shows simulation result for 100 cycles. (a) Phase variation. (b) Multitime solution of amplitude variation. (c) One-time solution of amplitude variation.

Now, note that the structure of $(\Omega(s) - \mathbb{T}_M)$ is as follows:

$$\begin{pmatrix} \ddots & & & & \\ & M+(s+j\omega_0)I & & & \\ & & M+sI & & \\ & & & M+(s-j\omega_0)I & \\ & & & & \ddots \end{pmatrix} \tag{32}$$

where

$$M = -\begin{pmatrix} 0 & & & \\ & \mu_2 & & \\ & & \ddots & \\ & & & \mu_n \end{pmatrix} \tag{33}$$

and I is the identity matrix of size $n \times n$ (n is the number of circuit unknowns).

$(\Omega(s) - \mathbb{T}_M)$ loses rank by one $\forall s = ij\omega_0$, so does $\overset{\text{HB}}{\mathbb{J}}(s)$. ■

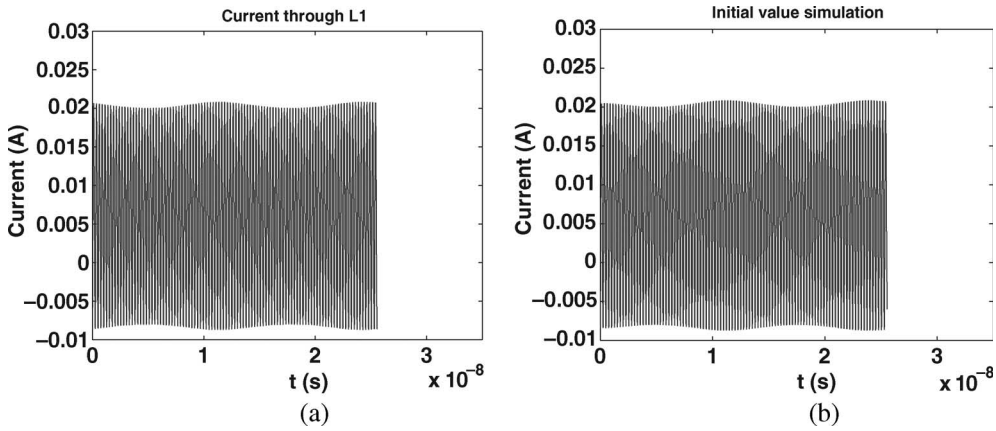

Fig. 16. Comparison of the result from small-signal analysis and full transient simulation [the perturbation current is $2 \times 10^{-3} \sin(1.02 w_0 t)$]. (a) Result recovered small-signal analysis. (b) Transient simulation result.

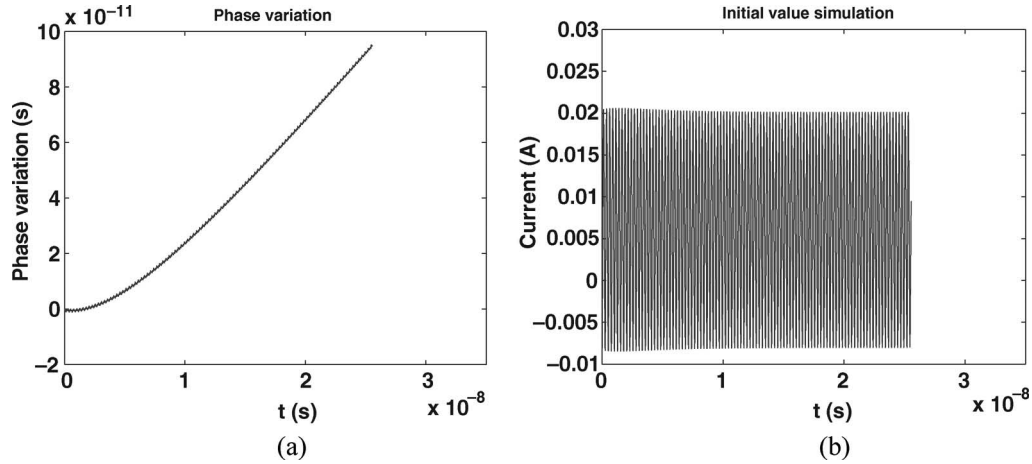

Fig. 17. Oscillator in lock: The perturbation current is $4 \times 10^{-3} \sin(1.005 w_0 t)$. The figure shows simulation result for 100 cycles. (a) Phase variation from small-signal analysis. (b) Transient simulation result.

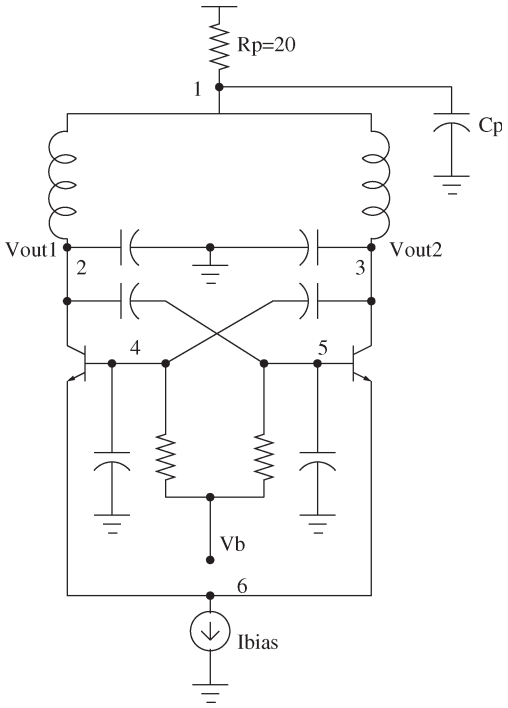

Fig. 18. One-GHz cross-coupled CMOS oscillator.

Lemma 2.2: Augmenting $\overset{\mathrm{HB}}{\mathbb{J}}(s)$ by a column $\overset{\mathrm{FD}}{\mathbb{V}}_{\dot{q}^*(t)}\left(\overset{\mathrm{HB}}{\mathbb{J}}_A(s)\right)$ restores full rank only in the case of $s = 0$.

Proof:

1) A vector can increase the rank of a rank-deficient matrix A only when it is not in the column space of A.
2) We need to show that $\overset{\mathrm{FD}}{\mathbb{V}}_{\dot{q}^*(t)} = \overset{\mathrm{HB}}{\mathbb{J}}(j\omega_0 i)x$ for some nonzero x and $\forall i \neq 0$. Or equivalently, using (31) that

$$\mathbb{T}_{V^{\mathrm{T}}(t)} \overset{\mathrm{FD}}{\mathbb{V}}_{\dot{q}^*(t)} = \mathbb{T}_{V^{\mathrm{T}}(t)} \mathbb{T}_{U(t)} \left(\Omega(j\omega_0 i) - \mathbb{T}_M\right) \mathbb{T}_{U(t)}^{-1} x$$

$$= \left(\Omega(j\omega_0 i) - \mathbb{T}_M\right) \mathbb{T}_{U(t)}^{-1} x. \tag{34}$$

3) We note that $\dot{q}^*(t) = C(t)\dot{x}_s^*(t)$. Hence, $\overset{\mathrm{FD}}{\mathbb{V}}_{\dot{q}^*(t)} = \mathbb{T}_C \mathbb{T}_U \overset{\mathrm{FD}}{\mathbb{V}}_{e_1}$ (see p used in [11, Remark II]). For ODE case, $\mathbb{T}_{V^{\mathrm{T}}(t)} \overset{\mathrm{FD}}{\mathbb{V}}_{\dot{q}^*(t)} = \mathbb{T}_{V^{\mathrm{T}}(t)} \mathbb{T}_U \overset{\mathrm{FD}}{\mathbb{V}}_{e_1} = \overset{\mathrm{FD}}{\mathbb{V}}_{e_1}$, and denote $\mathbb{T}_{U(t)}^{-1} x$ by y. Then, we have

$$\overset{\mathrm{FD}}{\mathbb{V}}_{e_1} = \left(\Omega(j\omega_0 i) - \mathbb{T}_M\right) y. \tag{35}$$

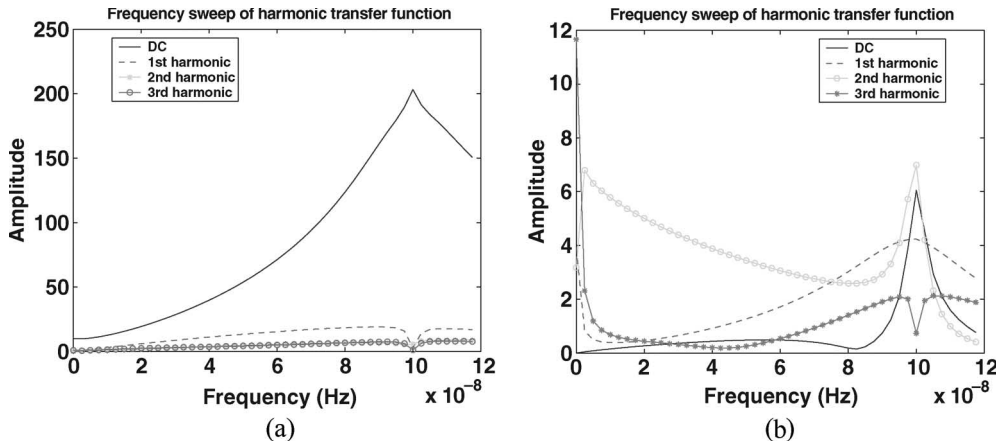

Fig. 19. Harmonic transfer functions: The frequency sweeps from dc to 1.2×10^9 Hz. (a) Harmonic transfer functions of the output voltage. (b) Harmonic transfer functions of the local frequency.

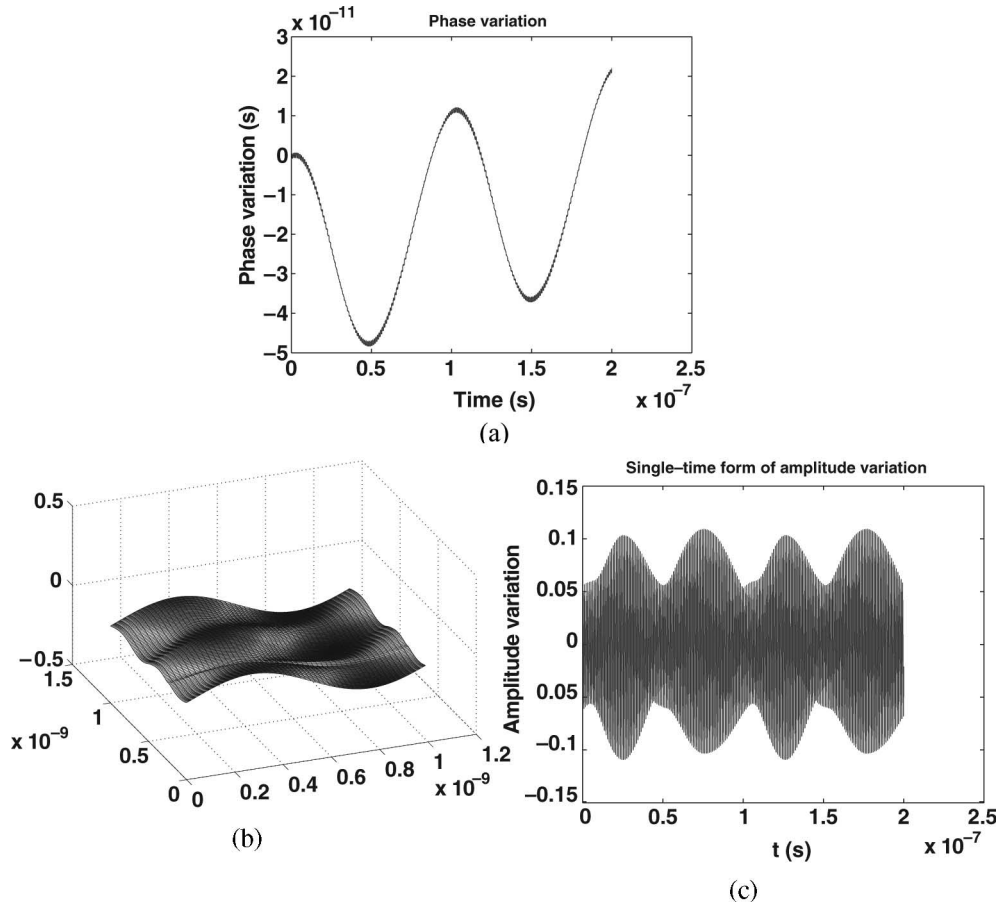

Fig. 20. Phase and amplitude variations of the output voltage when the perturbation current is $4 \times 10^{-4} \sin(1.01 w_0 t)$. The figure shows simulation result for 200 cycles. (a) Phase variation. (b) Multitime solution of amplitude variation. (c) One-time solution of amplitude variation.

From the structure of $(\Omega(j\omega_0 k) - \mathbb{T}_M)$ (32), we can see that $\mathbb{V}_{e_1}^{\mathrm{FD}}$ is in the span of $(\Omega(s) - \mathbb{T}_M)$ for any nonzero s (simply the first column of the middle block). Therefore, we can find a nonzero y solving the above for $s \neq 0$, and hence, a nonzero x. ■

Lemma 3.1: If $(\hat{\omega}, \hat{x})$ is a solution of (14), then the one-time waveform defined by $x(t) = \hat{x}(t, \hat{\phi}(t,t))$ solves the underlying DAE system if $b(t) = \hat{b}(t, \hat{\phi}(t,t))$, where $\hat{\phi}$ and $\hat{\omega}$ is related by

$$\frac{\partial \hat{\phi}(t,t)}{\partial t} = \frac{\partial \hat{\phi}(\tau_1 = t, \tau_2 = t)}{\partial \tau_1} + \frac{\partial \hat{\phi}(\tau_1 = t, \tau_2 = t)}{\partial \tau_2}$$

$$= \hat{\omega}\left(t, \hat{\phi}(t,t)\right).$$

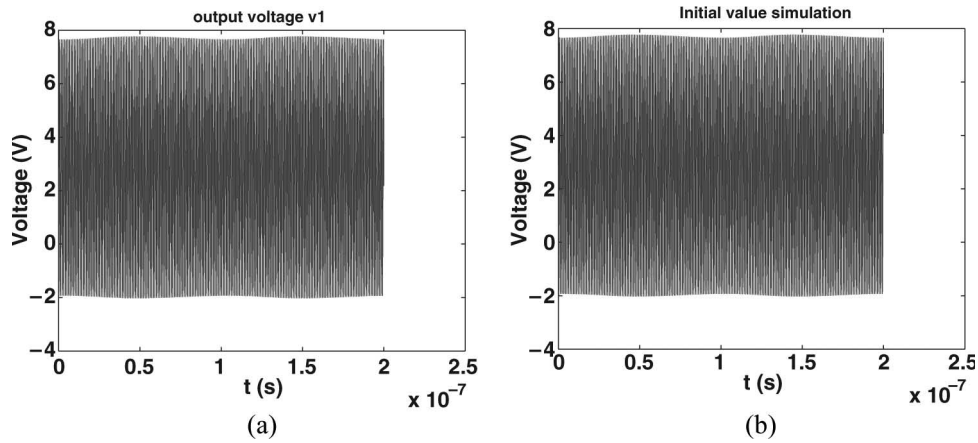

Fig. 21. Comparison of the result from small-signal analysis and full transient simulation [the perturbation current is $4 \times 10^{-4} \sin(1.01 w_0 t)$]. (a) Result recovered small-signal analysis. (b) Transient simulation result.

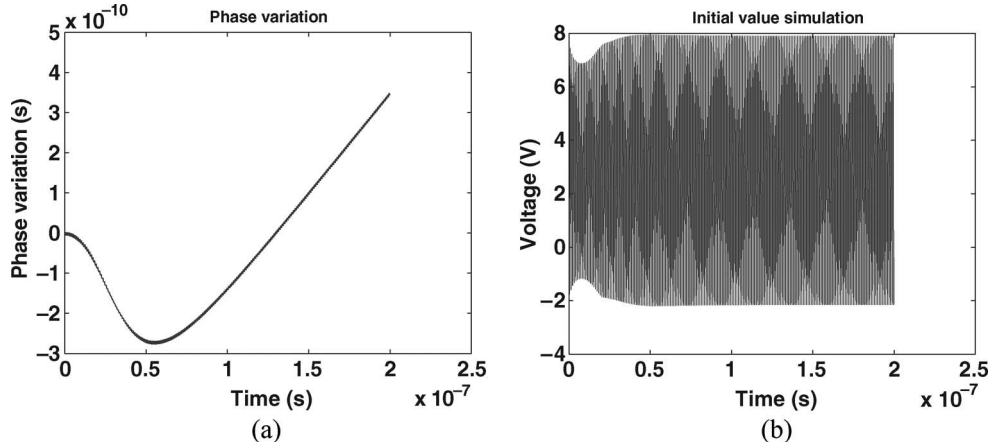

Fig. 22. Oscillator in lock: The perturbation current is $2 \times 10^{-3} \sin(1.005 w_0 t)$. The figure shows simulation result for 200 cycles. (a) Phase variation from small-signal analysis. (b) Transient simulation result.

Proof:

$$\begin{aligned}
\dot{q}\left(x(t)\right) &= \frac{\partial q\left(\hat{x}\left(t, \hat{\phi}(t,t)\right)\right.}{\partial t} \\
&= \frac{\partial q\left(\hat{x}\left(t, \hat{\phi}(t,t)\right)\right.}{\partial t_1} + \frac{\partial q\left(\hat{x}\left(t, \hat{\phi}(t,t)\right)\right.}{\partial t_2} \frac{\partial \hat{\phi}(t,t)}{\partial t} \\
&= \frac{\partial q\left(\hat{x}\left(t, \hat{\phi}(t,t)\right)\right.}{\partial t_1} + \frac{\partial q\left(\hat{x}\left(t, \hat{\phi}(t,t)\right)\right.}{\partial t_2} \\
&\quad \times \hat{\omega}\left(t, \hat{\phi}(t,t)\right) \\
&= -f\left(\hat{x}\left(t, \hat{\phi}(t,t)\right)\right. + \hat{b}\left(t, \hat{\phi}(t,t)\right) \\
&= -f(x) + b(t).
\end{aligned}$$

■

Lemma 3.2: The augmented matrix $\overset{\mathrm{HB}}{\mathbb{J}}_{\mathrm{Ge}}(s)$ (augmenting $\overset{\mathrm{HB}}{\mathbb{J}}(s)$ by columns of $\mathbb{T}_{\dot{q}^*(t_2)}$) is full rank at all frequencies.

Proof:

1) We only need to show that $\forall s = j\omega_0$, there is a vector (a column of $\mathbb{T}_{\dot{q}^*(t_2)}$) that is not in span of the column of $\overset{\mathrm{HB}}{\mathbb{J}}(s)$. Or equivalently, that there is a column z in $\mathbb{T}_{V^{\mathrm{T}}(t)} \mathbb{T}_{\dot{q}^*(t_2)}$ such that

$$z \neq \left(\Omega(j\omega_0 k) - \mathbb{T}_M\right) \mathbb{T}_U^{-1} x = \left(\Omega(j\omega_0 k) - \mathbb{T}_M\right) y. \tag{36}$$

2) For the ODE, $\mathbb{T}_{V^{\mathrm{T}}(t)} \mathbb{T}_{\dot{q}^*(t_2)} = \mathbb{T}_{V^{\mathrm{T}}(t)} \mathbb{T}_U \mathbb{T}_{e1} = \mathbb{T}_{e1}$. The structure of $\mathbb{T}_{e1}$ is

$$\begin{pmatrix} e1 & & & & \\ & \ddots & & & \\ & & e1 & & \\ & & & \ddots & \\ & & & & e1 \end{pmatrix}$$

where $e1 = [1, 0, \ldots, 0]^{\mathrm{T}}$ of size n.

From the structure of $(\Omega(j\omega_0 i) - \mathbb{T}_M)$ (32), we see that for $s = 0$, the middle column of $\mathbb{T}_{e_1}$ is not in the span of $(\Omega(s) - \mathbb{T}_M)$, for $s = -j\omega_0$, the column at the left of the middle column is not in the span of $(\Omega(s) - \mathbb{T}_M)$, etc.

Therefore, for all $s = \jmath\omega_0 i$, there is a column in $\mathbb{T}_{e_1}$ that is not in the span of $(\Omega(s) - \mathbb{T}_M)$, i.e., $\mathbb{T}_{e1}$ increase the rank of $\overset{\text{HB}}{\mathbb{J}}(s)$ by one. ■

Lemma 3.3: The phase-condition submatrix P is full rank at all frequencies.

Proof: Ω^{FD} loses rank by one, because Ω^{FD} has one zero term along the diagonal. When we augment Ω^{FD} with vectors which are columns of $\mathbb{T}_{\dot{x}^*(t_2)}$, there is at least one column in $\mathbb{T}_{\dot{x}^*(t_2)}$ that is not in the span of Ω^{FD} unless $\dot{x}_l^*(t_2) = 0$. We can always find nontrivial steady-state solutions $\dot{x}_l^*(t_2)$. Thus, augmenting Ω^{FD} with $\mathbb{T}_{\dot{x}_l^*(t_2)}$ restores full rank for the new phase-condition submatrix. ■

REFERENCES

[1] L. W. Nagel, "SPICE2: A computer program to simulate semiconductor circuits," Ph.D. dissertation, EECS Dept., Univ. California, Berkeley, Electron. Res. Lab., Berkeley, CA, 1975. Memo. ERL-M520.

[2] T. L. Quarles, *SPICE 3C.1 User's Guide*. Berkeley, CA: Univ. California, Berkeley, EECS Ind. Liaison Program, Apr. 1989.

[3] R. Telichevesky, K. Kundert, and J. White, "Receiver characterization using periodic small-signal analysis," in *Proc. IEEE Custom Integr. Circuits Conf.*, May 1996, pp. 449–452.

[4] R. Telichevesky, K. Kundert, and J. White, "Efficient ac and noise analysis of two-tone RF circuits," in *Proc. IEEE DAC*, 1996, pp. 292–297.

[5] M. Okumura, T. Sugawara, and H. Tanimoto, "An efficient small signal frequency analysis method of nonlinear circuits with two frequency excitations," *IEEE Trans. Comput.-Aided Design Integr. Circuits Syst.*, vol. 9, no. 3, pp. 225–235, Mar. 1990.

[6] M. Okumura, H. Tanimoto, T. Itakura, and T. Sugawara, "Numerical noise analysis for nonlinear circuits with a periodic large signal excitation including cyclostationary noise sources," *IEEE Trans. Circuits Syst. I, Fundam. Theory Appl.*, vol. 40, no. 9, pp. 581–590, Sep. 1993.

[7] A. Demir, A. Mehrotra, and J. Roychowdhury, "Phase noise in oscillators: A unifying theory and numerical methods for characterization," *IEEE Trans. Circuits Syst. I, Fundam. Theory Appl.*, vol. 47, no. 5, pp. 655–674, May 2000.

[8] X. Lai and J. Roychowdhury, "Automated oscillator macromodelling techniques for capturing amplitude variations and injection locking," in *Proc. IEEE ICCAD*, Nov. 2004, pp. 687–694.

[9] F. Kärtner, "Analysis of white and $f^{-\alpha}$ noise in oscillators," *Int. J. Circuit Theory Appl.*, vol. 18, no. 5, pp. 485–519, 1990.

[10] F. Kärtner, "Determination of the correlation spectrum of oscillators with low noise," *IEEE Trans. Microw. Theory Tech.*, vol. 37, no. 1, pp. 90–101, Jan. 1989.

[11] A. Demir and J. Roychowdhury, "A reliable and efficient procedure for oscillator PPV computation, with phase noise macromodelling applications," *IEEE Trans. Comput.-Aided Design Integr. Circuits Syst.*, vol. 22, no. 2, pp. 188–197, Feb. 2003.

[12] J. Roychowdhury, "Analyzing circuits with widely separated time scales using numerical PDE methods," *IEEE Trans. Circuits Syst. I, Fundam. Theory Appl.*, vol. 48, no. 5, pp. 578–594, May 2001.

[13] H. G. Brachtendorf, G. Welsch, R. Laur, and A. Bunse-Gerstner, "Numerical steady state analysis of electronic circuits driven by multitone signals," *Electr. Eng.*, vol. 79, no. 2, pp. 103–112, 1996.

[14] O. Narayan and J. Roychowdhury, "Analysing oscillators using multitime PDEs," *IEEE Trans. Circuits Syst. I, Fundam. Theory Appl.*, vol. 50, no. 7, pp. 894–903, Jul. 2003.

[15] R. Adler, "A study of locking phenomena in oscillators," *Proc. Inst. Radio Eng.*, vol. 34, no. 6, pp. 351–357, Jun. 1946.

[16] K. Kurokawa, "Injection locking of microwave solid-state oscillators," *Proc. IEEE*, vol. 61, no. 10, pp. 1336–1410, Oct. 1973.

[17] S. A. Maas, *Nonlinear Microwave Circuits*. Norwood, MA: Artech, 1988.

[18] K. Kurokawa, "Noise in synchronized oscillators," *IEEE Trans. Microw. Theory Tech.*, vol. MTT-16, no. 4, pp. 234–240, Apr. 1968.

[19] J. Roychowdhury, D. Long, and P. Feldmann, "Cyclostationary noise analysis of large RF circuits with multitone excitations," *IEEE J. Solid-State Circuits*, vol. 33, no. 3, pp. 324–336, Mar. 1998.

[20] K. Kundert, J. White, and A. Sangiovanni-Vincentelli, *Steady-State Methods for Simulating Analog and Microwave Circuits*. Norwell, MA: Kluwer, 1990.

Ting Mei (S'04) received the B.S. and M.S. degrees in electrical engineering from the Huazhong University of Science and Technology, Wuhan, China, in 1998 and 2001, respectively. She is currently working toward the Ph.D. degree in electrical engineering at the University of Minnesota, Twin City.

She is currently with the Electrical and Computer Engineering Department, University of Minnesota, Minneapolis. Her research interests include circuit- and system-level analysis and simulation of analog, RF, and mixed-signal systems.

Jaijeet Roychowdhury (S'85–M'94) received the B.S. degree in electrical engineering from the Indian Institute of Technology, Kanpur, India, in 1987, and the Ph.D. degree in electrical engineering and computer science from the University of California, Berkeley, in 1993.

From 1993 to 1995, he was with the Computer-Aided Design (CAD) Laboratory, AT&T Bell Laboratories, Allentown, PA. From 1995 to 2000, he was with the Communication Sciences Research Division, Bell Laboratories, Murray Hill, NJ. From 2000 to 2001, he was with CeLight Inc., an optical networking startup, Silver Spring, MD. Since 2001, he has been with the Electrical and Computer Engineering Department and the Digital Technology Center, University of Minnesota, Minneapolis. His professional interests include the design, analysis, and simulation of electronic, electrooptical, and mixed-domain systems, particularly for high-speed and high-frequency communication circuits.

Dr. Roychowdhury was an IEEE Circuits and Systems (IEEE CAS) Society Distinguished Lecturer during 2003–2005 and served as Program Chair of IEEE Technical Committee on Computer-Aided Network Design (CANDE) and behavioral modeling and simulation workshops (BMASs) in 2005. Currently, he serves on the Technical Program Committees of DAC, Design Automation and Test on Europe (DATE), ASP-DAC, IEEE International Symposium on Quality Electronic Design (ISQED), and BMAS, on the Executive Committee of ICCAD, on the Nominations and Appointments Committee of IEEE Council on Electronic Design Automation (CEDA), and as Treasurer of CANDE. He is the holder of ten patents. He was cited for Extraordinary Achievement by Bell Laboratories in 1996. Over the years, he has authored or coauthored five best or distinguished papers at Asia and South Pacific Design Automation Conference (ASP-DAC), Design Automation Conference (DAC), and International Conference on Computer-Aided Design (ICCAD).